PCCP

ROYAL SOCIETY OF CHEMISTRY

PAPER

View Article Online
View Journal | View Issue

Cite this: *Phys. Chem. Chem. Phys.*, 2020, **22**, 14077

The missing NH stretch fundamental in S_1 methyl anthranilate: IR-UV double resonance experiments and local mode theory†

Karl N. Blodgett,[a] Joshua L. Fischer,[a] Timothy S. Zwier‡*[a] and Edwin L. Sibert III*[b]

The infrared spectra of jet-cooled methyl anthranilate (MA) and the MA–H_2O complex are reported in both S_0 and S_1 states, recorded using fluorescence-dip infrared (FDIR) spectroscopy under jet-cooled conditions. Using a combination of local mode CH stretch modeling and scaled harmonic vibrational character, a near-complete assignment of the infrared spectra is possible over the 1400–3700 cm^{-1} region. While the NH stretch fundamentals are easily observed in the S_0 spectrum, in the S_1 state, the hydrogen bonded NH stretch shift is not readily apparent. Scaled harmonic calculations predict this fundamental at just below 2900 cm^{-1} with an intensity around 400 km mol^{-1}. However, the experimental spectrum shows no evidence of this transition. A local mode theory is developed in which the NH stretch vibration is treated adiabatically. Minimizing the energy of the corresponding stretch state with one quantum of excitation leads to a dislocation of the H atom where there is equal sharing between N and O atoms. The sharing occurs as a result of significant molecular arrangement due to strong coupling of this NH stretch to other internal degrees of freedom and in particular to the contiguous HNC bend. A two-dimensional model of the coupling between the NH stretch and this bend highlights important nonlinear effects that are not captured by low order vibrational perturbation theory. In particular, the model predicts a dramatic dilution of the NH stretch oscillator strength over many transitions spread over more than 1000 cm^{-1}, making it difficult to observe experimentally.

Received 8th April 2020,
Accepted 13th June 2020

DOI: 10.1039/d0cp01916j

rsc.li/pccp

I. Introduction

Excited state intramolecular hydrogen atom (or proton) transfer followed by internal conversion and subsequent hydrogen atom back-transfer is the regenerative mechanism by which many UV-absorbing sunscreen agents are understood to act.[1–7] Alternatively, as is the case for salicylic acid and its derivatives, excited state H-atom transferred products can undergo radiative decay to the ground state, which is detectable by its characteristic Stokes-shifted emission.[2,3,8,9]

Rather than full H-atom transfer, anthranilic acid (AA) has been described as undergoing hydrogen atom dislocation in the S_1 electronic state. This process is characterized by the strengthening of the 6-membered intramolecular HNH···O=C hydrogen bond and was initially diagnosed in 2004 by Southern *et al. via* AA's infrared (IR) spectrum in the hydride stretch region.[10] The authors reported that the coupled NH_2 group vibrations in S_0 appeared to uncouple from one another in S_1 and present as a 'free' NH stretch (3460 cm^{-1}) and a weak, broadened, redshifted 'dislocated' NH stretch centered at 2900 cm^{-1}. Shortly after, Sobolewski *et al.* published time-dependent density functional theory (TD-DFT) harmonic vibrational frequencies in the S_0 and S_1 electronic states of AA.[11] The S_1 frequencies agreed well with the experimental values, but the dislocated NH stretch intensity was calculated to be orders of magnitude larger than its experimentally assigned value. This intensity mismatch persists, with a recent computational study by Egidi *et al.* using second-order vibrational perturbation theory (VPT2) to calculate the excited state IR spectrum of AA, yielding qualitatively similar results.[12]

We have recently published results on the vibronic spectroscopy of jet-cooled methyl anthranilate (MA), the methyl ester of AA, and its water complex (MA–H_2O).[13] Long Franck–Condon progressions of in-plane modes indicate significant heavy-atom

[a] *Department of Chemistry, Purdue University, West Lafayette, IN 47907-2084, USA. E-mail: tszwier@sandia.gov*
[b] *Department of Chemistry, University of Wisconsin-Madison, Madison, WI 53706, USA. E-mail: elsibert@wisc.edu*

† Electronic supplementary information (ESI) available: Calculated electronic states in MA and MA–H_2O, electrostatic potential mapped onto increasing electron density surface in MA–H_2O, NH and ND stretch eigenfunctions and corresponding potentials in the S_1 state. See DOI: 10.1039/d0cp01916j

‡ Current address: Combustion Research Facility, Sandia National Laboratories, Livermore, CA 94551, USA.

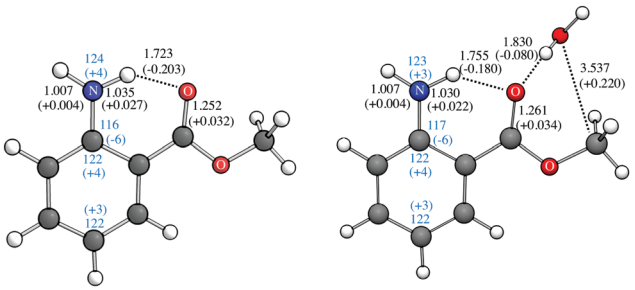

Fig. 1 S_1 excited state optimized geometries of (left) methyl anthranilate and (right) its water complex. Bond distances are labelled in black text and angles in blue text. Changes in these parameters from their ground state values are shown in parentheses. Adapted from *Phys. Chem. Chem. Phys.*, 2019, **21**, 21355 with permission of the PCCP Owner Societies.

rearrangement between the S_0 and S_1 electronic states. Accompanying these large geometry changes is extensive Duschinsky mixing involving both the in-plane and out-of-plane vibrations. Corroborating computational evidence (TD-DFT B3LYP-D3BJ/def2TZVP) indicates that the 6-membered HNH···O=C hydrogen bond distance decreases by 0.203 Å (from 1.926 Å to 1.723 Å). Fig. 1 presents the assigned, calculated S_1 geometries of MA and MA–H_2O, labelled with important structural parameters and their changes from S_0 (shown in parentheses). The strengthening of the H-bond results from an extensive reorientation of the NH_2 and CO_2Me groups. These structural parameters are similar to those calculated for AA.[11,12,14]

In this manuscript we expand upon our recent study by presenting the ground and excited state IR spectrum of MA and MA–H_2O in the hydride stretch (2400–3800 cm^{-1}) and mid-IR (1400–1800 cm^{-1}) regions. With firm structural assignments in hand, we further characterize the H-atom dislocation from both the donor and acceptor's perspective. Using a local mode Hamiltonian in conjunction with DFT frequency calculations, we firmly assign all IR transitions the hydride stretch region in the S_0 and S_1 states of MA and MA–H_2O. With all transitions accounted for, we propose a novel explanation for the discrepancy between experimental and calculated intensity of the dislocated NH stretch transition, based on the adiabatic separation of the NH stretch and other internal coordinates.

II. Experimental methods

Methyl anthranilate (MA) was purchased from Sigma-Aldrich (≥99% purity) and used without further purification. MA was seeded in Helium and pulsed (Parker General Valve Series 9) into a vacuum chamber, resulting in a free jet expansion. Trace water in the sample was sufficient for producing water complex population for fluorescence measurements while ~5% water was flowed over the ~65 °C heated MA reservoir to create sufficient MA–H_2O complexes for ionization measurements. Both the laser-induced fluorescence and laser ionization/time-of-flight mass spectrometer chambers used to collect data have been described previously.[15,16] UV light was generated with nanosecond Nd:YAG-pumped dye lasers (Radiant Dyes NarrowScan and Lambda Physik ScanMate Pro), while a Nd:YAG pumped KTA-based optical parametric converter (LaserVision) was used as the tunable IR source.

Species-specific infrared spectra in the hydride stretch region (2400–3800 cm^{-1}) were recorded using fluorescence dip infrared (FDIR) spectroscopy.[17] Collection of a ground state FDIR spectrum requires a scanning IR holeburn laser (10 Hz) and a UV probe laser (20 Hz) which is fixed on some intense vibronic transition. The IR laser temporally precedes (~100 ns) the UV laser so that when the IR laser is resonant with the same species as the UV laser, population is removed from the ground state vibrational zero-point level, producing a depletion in the fluorescence intensity. Plotting the fluorescence depletion as a function of IR wavelength yields the ground state FDIR spectrum. Collection of excited-state FDIR spectra requires different laser timings. In this scheme, the fixed UV laser precedes the scanning IR laser by ~10 ns. When the IR laser is resonant with a vibrational transition of the electronically excited molecule, the rate of non-radiative decay is increased relative to that of the initially excited level, resulting in a dip in fluorescence signal. The excited-state FDIR spectrum results from plotting the fluorescence depletion against the IR wavelength.

Species-specific infrared spectra in the mid-IR region (1400–1800 cm^{-1}) were recorded using resonant ion-dip infrared (RIDIR) spectroscopy.[17] The scheme for collecting ground state RIDIR spectra is nearly identical to that for collecting the corresponding FDIR spectra, except ion signal instead of fluorescence is measured. The ionization potential of MA and MA–H_2O are such that a second shorter wavelength laser is needed to ionize out of the prepared electronically excited states. Maximum ion signal is obtained with temporally overlapped UV lasers. Collection of excited state RIDIR spectra requires the temporal separation of the excitation and ionization laser by ~16 ns so that the scanning IR laser can arrive between them. When the IR laser is resonant with an excited state vibrational transition the molecule accesses levels that decrease the ionization efficiency, *e.g.* through internal conversion or dissociation. When this occurs, fewer ions are generated, resulting in a dip in ion signal.

III. Computational methods

Standard harmonic and anharmonic vibrational frequency calculations were performed with Gaussian16[18] *via* (TD-)DFT using the B3LYP hybrid functional in conjunction with Grimme's dispersion correction (version D3),[19] Becke–Johnson damping,[20] and the def2TZVP basis set. Frequencies in the amide I and II regions (1400–1800 cm^{-1}) were scaled by a factor of 0.984 and compared directly with experiment.

The theoretical results include both ground and excited state calculations of the XH stretch vibrations (X = N, C, and O). We group the calculations into two areas. In the first, we apply a local model CH stretch Hamiltonian with extensions for the descriptions of the NH and OH stretches in order to describe the vibrational band positions of all the XH stretch vibrations,

and make comparisons with experiment. In the second we develop a model for the missing NH stretching vibration predicted to occur around 2900 cm^{-1} in normal mode and VPT2 calculations.

A. Description of the local mode Hamiltonians

We model the CH stretch region of the IR spectra following the method of Tabor *et al.*[21] In this approach, localized CH stretch vibrations couple *via* 2 : 1 Fermi resonances to scissor vibrations. The localization of these modes follows from taking suitable linear combinations of the normal modes to obtain a quadratic, local mode Hamiltonian

$$H = \frac{1}{2}\sum_{i=1}^{N} P_i^2 + \frac{1}{2}\sum_{i=1}^{N}\sum_{j=1}^{N} F_{ij}R_iR_j. \quad (1)$$

Details of this localization procedure are provided in the Appendix.

To account for diagonal anharmonicity and the modest level of theory, the frequencies of the uncoupled normal modes are then scaled, where the scale factor depends on the level of theory used in the electronic structure normal mode calculation. Select anharmonic terms, calculated for a model system, are added to the Hamiltonian. These terms lead to shifts and couplings between stretch states with one quantum of excitation and scissor states with two quanta of excitation. The dipole moment is taken as the linear dipole moment calculated *ab initio*.

The scaling factors of the OH stretches in the MA–H_2O complex were obtained by scaling the localized normal mode frequencies to best match the local mode OH stretch fundamentals obtained from the Paesani water potential for the book conformer of $(H_2O)_6$. To obtain these latter energies, which are based on a potential of CCSD(T)/pVTZ quality, we calculated sixth-order three-dimension stretch–bend localized normal coordinate force fields for each water molecule of the book conformer, constraining the remaining degrees of freedom to the equilibrium geometries. We then carried out 4th order CVPT calculations to obtain effective Hamiltonians describing the anharmonic OH stretches, the scissor overtones, and the coupling between them. We denote the 12 transition energies of the OH stretches as $\tilde{\nu}^{P}$. We then calculated the 12 localized normal coordinate transition energies $\tilde{\nu}_{local,calc}$ for the book conformer at the harmonic level using the B3LYP/def basis set whose results we wish to scale. The scale factors are obtained *via* a least squares fit, $\tilde{\nu}_{local,f} = A\tilde{\nu}_{local,calc} + B$, to obtain the best fit to the $\tilde{\nu}^{P}$ values. The fit parameters are A = 0.8464 and B = 457.4 cm^{-1}.

The NH stretch fundamentals were scaled by a multiplicative factor of 0.957 to match the NH stretch fundamentals (3390/3540 cm^{-1}) of the S_0 state of the monomer.

B. Theoretical modeling of the NH stretch fundamentals

As we shall see, the differences between the theoretical and experimental results for the hydrogen bonded NH stretch are profound at the harmonic level. These differences persist even when anharmonicities are taken into account. Studies of anthranilic acid (AA) provide a good point of comparison. AA has a carboxylic acid group (COOH) that becomes a methyl ester in methyl anthranilate (COOMe). Second order perturbation studies of the vibrations on the S_1 electronic state have been carried out by Egidi *et al.*[12] These calculations, based on TDDFT with a B3LYP/SSND basis, predict a very intense H-bonded NH stretch peak around 2800 cm^{-1}. The authors note the discrepancy between theory and experiment, and point to the need for further studies. In the present modeling, we consider two theoretical approaches that extend beyond the perturbative approach in order to examine the role of anharmonic effects. These studies include an adiabatic treatment of the NH stretch and a reduced two-dimension grid-based study of the NH stretch–bend coupling.

1. NH stretch vibrationally adiabatic surface determination. To find the adiabatic surfaces for the NH stretch vibrational levels, we use optimization approaches similar to those used in electronic structure theory. In such calculations, one inputs an initial geometry and then searches for a minimum using gradients and, if needed, second derivatives. The only difference here is that the NH stretch is also treated quantum mechanically.

In order to calculate the forces and the Hessian, for a given geometry, we use an electronic structure program to provide

$$F_i = -\frac{\partial V}{\partial x_i}; \quad H_{ij} = \frac{\partial^2 V}{\partial x_i \partial x_j}. \quad (2)$$

The forces and Hessian are transformed to a set of internal coordinates $\mathbf{x} = \mathbf{B}^{-1}\mathbf{S}$ that are comprised of stretches, angles, and dihedral angles. The elements of the B-inverse matrix $B_{ki}^{-1} = \frac{\partial x_k}{\partial S_i}$ and its higher order derivatives follow from the geometrical transformation between the internal coordinates in a given body-fixed frame and the Cartesian coordinates. Calculating these elements using finite difference methods, we determine the internal forces

$$f_i = -\frac{\partial V}{\partial S_i} = -\sum_k \frac{\partial x_k}{\partial S_i}\frac{\partial V}{\partial x_k} \quad (3)$$

and Hessian

$$h_{ij} = \frac{\partial^2 V}{\partial S_i \partial S_j} = -\sum_k \frac{\partial^2 x_k}{\partial S_i \partial S_j}F_k + \sum_{kl}\frac{\partial x_k}{\partial S_i}\frac{\partial x_l}{\partial S_j}H_{kl}. \quad (4)$$

We assume that $R = S_1$ corresponds to the NH stretch of interest and use eqn (3) and (4) to expand the potential to second-order in the remaining internal extension coordinates

$$V(R,S) = V(R) - \sum_i f_i(R)S_i + \frac{1}{2}\sum_{ij} h_{ij}(R)S_iS_j. \quad (5)$$

Here the summations are from $i = 2$ to $3N - 6$ where N is the number of atoms. In order to obtain the variables of eqn (5) as a function of R, we carry out electronic structure calculations of the energy, force and Hessian keeping all the internal coordinates fixed except for R. This internal coordinate is evaluated at a set of equally space grid points that form the basis of a

subsequent discrete variable representation (DVR) calculation. We solve for the NH stretch eigenfunctions by carrying out this DVR calculation using the stretch Hamiltonian.

$$[\hat{T}_R + V(R,S=0)]\Psi_n(R) = E_n(\boldsymbol{S})\Psi_n(R). \quad (6)$$

Here the kinetic contribution uses the reduced mass of the NH oscillator.

In order to minimize the energy $E_n(\boldsymbol{S})$ with respect to the remaining degrees of freedom for a given value of n, we calculate the Hellman–Feynman forces

$$\frac{\partial E_n}{\partial S_j} = \int dR \Psi_n \times \frac{\partial \hat{H}}{\partial S_j} \Psi_n = -f_{nn}^j \quad (7)$$

where

$$f_{nm}^j = \int dR \Psi_n \times f_j(R) \Psi_m. \quad (8)$$

These matrix elements are easily evaluated in the DVR representation by summing over the contributions at the DVR points. The components of this calculation are shown in Fig. 2 for the force along the HNC angle and the first excited state of the NH stretch.

Combining these first derivatives with similarly calculated second derivatives allows us to estimate the changes in the values of the internal coordinates that minimize the NH stretch energy. In practice we had to repeat this process 11 times in order to find the minimum, due to the presence of higher order terms not included in eqn (5). Fig. 2 shows the components of eqn (8) that are needed to carry out the integration in the DVR. The figure shows results for the second-to-last step in the minimization process. For this step, the expectation value of the force along the HNC angle with respect to $\Psi_1(R)$ has been reduced to 60 cm^{-1} per rad. This small residual force led to predicted shift in the HNC angle of only 0.0008 rad. In the subsequent step of the minimization these two values reduce to an average force of 1.4 cm^{-1} per rad and a predicted step size of 0.00001 rad. Consequently, the calculation was assumed to be converged. All other average forces at the minimum were smaller in magnitude. The noteworthy feature of the figure is that the force is highly nonlinear over the large expanse of the NH stretch coordinate for which the wave function has appreciable amplitude.

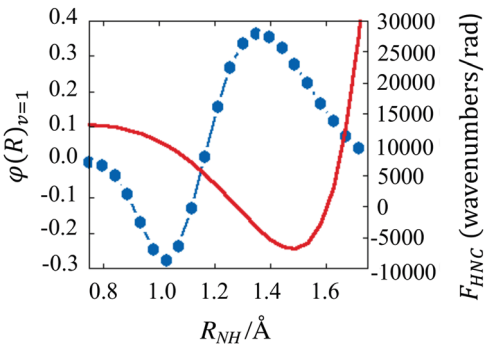

Fig. 2 The $\Psi_1(R)$ wavefunction (dotted blue line) of eqn (6) plotted as a function of NH stretch bond length R (in Angstroms). Remaining coordinates are chosen to minimize the energy corresponding to this state. The points correspond to the centers of the DVR sinc functions used in the minimization. The solid red line is the force along the HNC angle in cm^{-1} per rad as a function of R.

2. Description of the reduced-dimension stretch–bend Hamiltonian. The mode most strongly coupled to the NH stretch is the contiguous HNC bend. We solved the Schrodinger equation for these two degrees of freedom assuming that the remaining coordinates are constrained to the geometry that minimizes the $\nu_{NH} = 0$ state following the procedure described above. The eigenfunctions and eigenvalues are obtained using a two-dimensional DVR calculation following the DVR procedure outlined by Luckhaus.[22] When focusing on the S_1 state NH stretch transitions, the input data for the calculation are the potential points for the S_1 surface calculated on a 20 × 20 grid of points obtained at the B3LYP/6-311++(d,p) level of theory with Grimme's empirical dispersion.[19] The g-matrix elements are evaluated numerically at each of these points following the methods of Wilson, Decius, and Cross for constrained systems.[23] The advantage of the Luckhaus approach is that it allows us to incorporate the coordinate dependence of the g-matrix in a straightforward way as well as include the stretch–bend couplings in the kinetic energy contribution to the Hamiltonian.

IV. Results

A. Methyl anthranilate monomer

The assigned FDIR spectrum in the hydride stretch region of MA in the ground electronic states is shown in Fig. 3a. Three distinct sets of fundamental vibrational transitions appear, due to the NH_2, aromatic CH, and methyl CH stretches, the last of which is replete with 2 : 1 Fermi resonance contributions with the CH scissor overtones. The stick diagram below the experimental spectrum displays the results of the local mode anharmonic modeling. The match between experiment and theory is excellent, with an average error of 4 cm^{-1} (Table 1).

The bands at 3540 and 3390 cm^{-1} are assigned to the coupled NH stretch modes of the NH_2 group. In the ground state, these two fundamentals are best described as asymmetric and symmetric stretch fundamentals, respectively, despite the presence of the H-bond involving one of the NH bonds. This perturbation results in mixing coefficients of $\alpha = -0.47$ and $\beta = 0.88$ for the NH groups in the coupled NH_2 vibrations. In aniline, the unperturbed SS and AS fundamentals appear at 3508 and 3422 cm^{-1}, respectively.[24] The weak transition just on the high frequency side of the symmetric stretch NH_2 fundamental (marked with a dagger) is likely the result of a 2 : 1 Fermi resonance between the NH_2 SS fundamental and the C=O stretch overtone, while the band at 3303 cm^{-1} (marked with a double dagger) is likely the NH_2 bend overtone.

The peaks (shaded in red) in the spectrum are due to Fermi resonance-mixed methyl CH stretch transitions. Note the excellent fit between experiment and the local mode theory (Section III.A). That band intensities in this region of the spectrum are comparable to those in the NH stretch region is

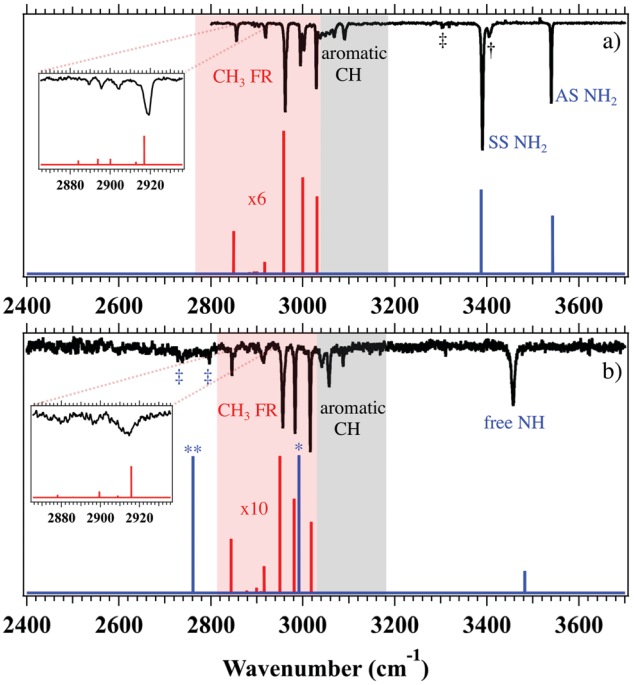

Fig. 3 (a) Ground and (b) S_1 excited state FDIR spectra of methyl anthranilate from 2400–3700 cm^{-1}. The spectra are divided into four regions, from high to low frequency: NH stretch (not shaded), aromatic CH stretch (shaded in grey), CH_3 stretch (shaded in red), and low frequency (not shaded). The experimental spectrum (black trace) is compared with the predictions of local mode modeling (unmarked stick spectra) in both electronic states. Sticks colored in blue correspond to NH_2 vibrations while those in red are due to CH_3 vibrations. The transition marked with a dagger in (a) is likely a result of 2 : 1 Fermi resonance between the SS NH_2 and C=O stretch overtone, while the band marked with a double dagger is likely the NH_2 bend overtone. Peaks marked with double daggers in (b) are low-intensity bands. In both states the red stick spectra corresponding to the CH_3 Fermi-mixed transitions have been multiplied by a single scale factor for comparison with experiment. The blown-up regions show the excellent fit of the Fermi-mixed CH_3 stretch transitions with local mode modeling. The blue stick in (b) with a single asterisk at 2991 cm^{-1} is the calculated harmonic dislocated NH stretch while the blue stick marked with a double asterisk at 2761 cm^{-1} is the calculated standard anharmonic dislocated NH stretch transition. See text for further discussion.

due to saturation effects at the IR laser powers used to record the spectra. The transitions from ~3030–3100 cm^{-1} belong to aromatic CH stretch transitions, which are coupled *via* resonances with ring CH bend modes.[25] We have made no attempt to fit the aromatic CH stretches.

Fig. 3b shows the S_1 state FDIR spectrum over the 2400–3700 cm^{-1} region. The high frequency region differs substantially from that of the ground state. We observe a single band at 3457 cm^{-1} with a FWHM of 8 cm^{-1}, nearly double the width of the ground state NH stretch transitions. S_1 normal mode calculations at the B3LYP-D3BJ/def2TZVP level indicate that this vibration is localized almost entirely on the free NH bond, indicating that the NH_2 group vibrations have almost completely decoupled from one another due to the NH···O=C H-bond. The intense transition just below 3000 cm^{-1} in blue in Fig. 3b (single asterisk) is that predicted for the H-bonded, 'dislocated' NH stretch fundamental in S_1 by harmonic calculations at the same level of theory (with the same scale factor as for the free NH stretch). When standard corrections due to anharmonicity are included, the frequency of this transition is lowered to 2761 cm^{-1} (double asterisk), with no scale factor applied. In both cases, this transition is calculated to be more than ten times more intense than all other transitions in the region.

Notably, all the peaks in the methyl CH stretch region (2800–3000 cm^{-1}, red sticks) are firmly assigned to the methyl group by the CH stretch local mode Fermi resonance model. The ability of the model to account quantitatively for all observed transitions in this region makes the absence of a high intensity experimental NH stretch transition all the more conspicuous. While the region from 2400–2800 cm^{-1} does contain some broad, weak bands (marked with blue double daggers), we note the absence of a well-resolved intense transition. We return to this point later in the discussion.

The S_0 and S_1-state IR spectra of MA in the 1400–1800 cm^{-1} regions are shown in Fig. 4a and b, respectively. We anticipate the presence of strong IR transitions in this region due to the C=O stretch and NH_2 scissor fundamentals. In the ground electronic state, the carbonyl stretch fundamental appears as the intense peak at 1721 cm^{-1}, while the NH_2 bend is observed at 1632 cm^{-1}. Already in the ground state, these transitions appear at frequencies that reflect a substantial NH···O=C H-bond, lowering the frequency of the ester C=O stretch fundamental and raising the frequency of the NH_2 bend relative to their counterparts in the absence of a hydrogen bond between them. For instance, the corresponding C=O stretch and NH_2 bend transitions in benzoic acid (free C=O group) and aniline (free NH_2 group) are at 1752 and 1623 cm^{-1}, respectively.[26–29]

The excited state spectrum shows a broadened C=O stretch transition at 1637 cm^{-1}, shifted 83 cm^{-1} lower in frequency than its ground state counterpart. The NH_2 bend shows a similar redshift of 76 cm^{-1} to 1557 cm^{-1} in S_1. While captured by the calculations, the shift of the NH_2 bend to lower frequency upon $\pi\pi^*$ excitation is surprising, because the NH_2 group is engaged in a stronger H-bond to C=O in the S_1 state, which typically would raise the frequency of the NH_2 bend. These substantial frequency shifts upon electronic excitation reflect both the extensive heavy-atom rearrangement and subsequent change in hydrogen bonding strength from both the acceptor and donor's point of view, both of which are facilitated by the shifting electronic charge upon excitation. Fig. 5 presents the calculated change in electrostatic potential mapped onto the surface of increasing electron density in going from S_0 to S_1. There is a significant shift in electron density/negative charge from the NH_2 to the carbonyl group upon electronic excitation, much as one might expect of a proton-coupled electron transfer. Here, however, the transfer is incomplete, but the charge redistribution nevertheless represents a substantial increase in hydrogen bond strength on the S_1 surface. As we shall see shortly, the

Table 1 Select experimental and calculated frequencies in MA

S_0			S_1		
Exp./cm^{-1}	Calc./cm^{-1}	Assignment	Exp./cm^{-1}	Calc./cm^{-1}	Assignment
3540	3543^c (3540^a)	NH_2 AS stretch	3457	3482^c (3483^a)	'Free' NH stretch
3390	3388^c (3387^a)	NH_2 SS stretch	2600–2800	2991^c (2991^a), (2761^b)	'Dislocated' NH stretch
3029	3031^c (3021^a)	CH_3 FR	3016	3018^c (3007^a)	CH_3 FR
3002/2995	3000^c (2989^a)	CH_3 FR	2983	2981^c (2970^a)	CH_3 FR
2962	2958^c (2924^a)	CH_3 FR	2956	2950^c (2912^a)	CH_3 FR
2919	2917^c	CH_3 FR	2914	2916^c	CH_3 FR
2913	2913^c	CH_3 FR	—	2909^c	CH_3 FR
2904	2900^c	CH_3 FR	2896	2899^c	CH_3 FR
2896	2894^c	CH_3 FR	—	2886^c	CH_3 FR
2889	2884^c	CH_3 FR	2880	2878^c	CH_3 FR
2856	2849^c	CH_3 FR	2845	2844^c	CH_3 FR
1720	1697^a	C=O stretch	1637	1636^a	C=O stretch
1632	1632^a	NH_2 bend	1557	1535^a	NH_2 bend

^{a} Scaled harmonic frequency. ^{b} Anharmonic frequency. ^{c} Frequency from local mode model.

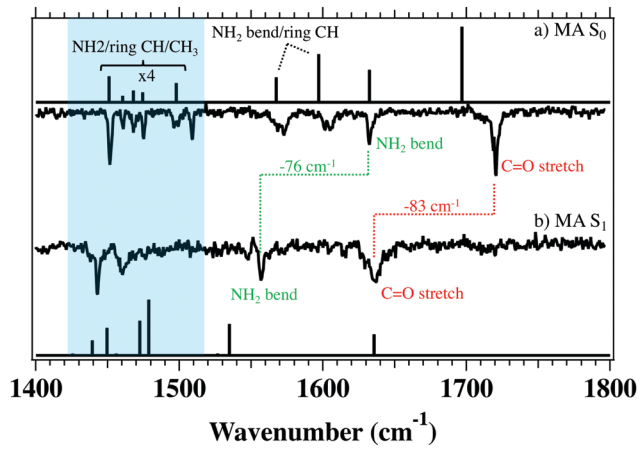

Fig. 4 (a) Ground and (b) S_1 excited state RIDIR spectra of methyl anthranilate from 1400–1800 cm^{-1}. The calculated scaled harmonic normal mode frequencies (black stick spectra) are compared with experiment. See text for further discussion.

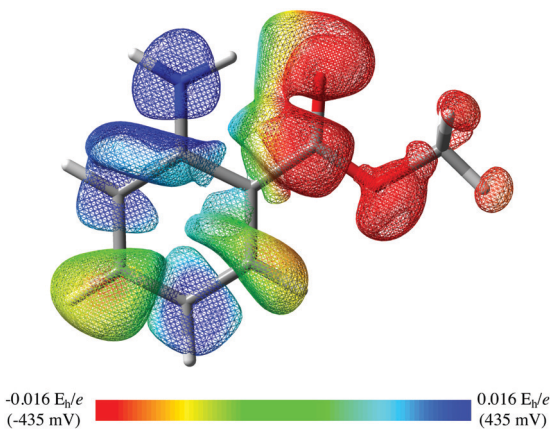

Fig. 5 The change in electrostatic potential mapped onto the surface of increasing electron density in going from S_0–S_1 in methyl anthranilate. Calculated at the TD-DFT B3LYP-D3BJ/def2TZVP level of theory.[18]

degree to which H-atom transfer occurs depends sensitively on NH stretch vibrational excitation.

B. MA–H_2O complex

The corresponding S_0 and S_1-state FDIR spectra of the MA–H_2O complex in the hydride stretch region are shown in Fig. 6a and b. The stick diagram below the experimental spectrum displays the results of the local mode anharmonic modeling. The match between experiment and theory is excellent, with an average error of 8.5 cm^{-1} (Table 2). The S_0 asymmetric and symmetric NH_2 stretches appear at 3543 and 3405 cm^{-1}, respectively. The smaller splitting of these coupled stretches relative to that in the monomer reflects the weaker NH$\cdots$O=C hydrogen bonding strength in the water complex as a result of the carbonyl acting as a dual H-bond acceptor. The two higher frequency transitions at 3725 and 3569 cm^{-1} belong to the asymmetric and symmetric H_2O vibrations, respectively. The aromatic CH and fit Fermi-coupled CH_3 regions show similar structure to that found in the monomer spectrum.

The high frequency region of the S_1 MA–H_2O spectrum (Fig. 6b) is markedly different from the ground state spectrum above it. The tiny peaks marked with daggers are small contributions from the S_0 MA–H_2O spectrum, which appear as a result of the slight overlap of the UV and IR lasers necessitated by a short excited state lifetime (23 ns). In the S_1 state spectrum, the asymmetric and symmetric water stretch transitions are at 3721 and 3516 cm^{-1}, respectively, the latter of which is shifted 53 cm^{-1} lower in frequency than in the ground state. This shift is indicative of an increasing OH$\cdots$O=C hydrogen bond strength, as supported by the assigned geometry (Fig. 1) and the calculated shortening of the OH$\cdots$O=C H-bond length (by 0.080 Å) upon electronic excitation (Fig. 1b). Much as in the monomer ground state spectrum, a band with FWHM of 7 cm^{-1} at 3461 cm^{-1} is assigned to the free NH stretch of the uncoupled NH_2 group. The calculated, intense transition (blue stick) marked with an asterisk at 3072 cm^{-1} is due to the H-bonded 'dislocated' NH stretch transition, which is absent from the experimental spectrum in both frequency position and intensity. Indeed, the local mode modelling of the CH_3 stretches firmly assigns all experimental bands to Fermi-coupled states in this region, as it did in the MA monomer. This leaves all observed bands accounted for except for the

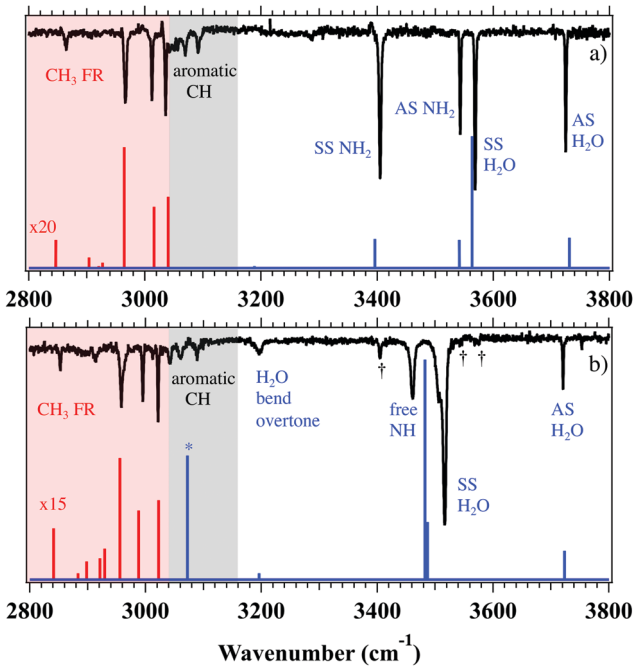

Fig. 6 (a) Ground and (b) S_1 excited state FDIR spectra from 2800–3800 cm^{-1} of the methyl anthranilate–H_2O complex. The spectra are divided into three regions: NH stretch (not shaded), aromatic CH stretch (shaded in grey), and CH_3 stretch (shaded in red). The experimental spectrum (black trace) is compared with the predictions of local mode modeling (unmarked stick spectra) in both electronic states. Stick spectra colored in blue correspond to NH_2 and H_2O vibrations while stick spectra colored in red correspond to CH_3 vibrations. The transitions marked with daggers in (b) are small contributions from the S_0 MA–H_2O spectrum, which appear as a result of the slight overlap of the UV and IR lasers necessitated by a short excited state lifetime (23 ns). In both states the red stick spectra corresponding to the CH_3 Fermi-mixed transitions have been multiplied by a scale factor for a more ready comparison with experiment. The blue stick in (b) with a single asterisk at 3072 cm^{-1} is the calculated harmonic dislocated NH stretch transition. See text for further discussion.

14 cm^{-1} FWHM peak at 3196 cm^{-1}, which according to our local mode modelling is the H_2O bend overtone.

The S_0-state mid-IR spectrum of MA–H_2O is presented in Fig. 7a. The C═O stretch fundamental of the water complex appears at 1702 cm^{-1}, shifted 18 cm^{-1} to lower frequency than in the monomer. This frequency shift reflects that the C═O group is accepting an additional H-bond from the water OH group. The NH_2 bend appears at 1634 cm^{-1}, nearly the same frequency as its monomer counterpart. This unperturbed band position provides evidence that the H_2O molecule is not interacting directly with the amine group, conforming our assigned structure (Fig. 1b).

The mid-IR spectrum in the S_1 state reflects the general structural change present in the monomer, modified by the H_2O molecule forming a second H-bond to the C═O group. For instance, the C═O stretch transition in S_1 MA–H_2O is shifted down in frequency relative to S_0 by 91 cm^{-1} to 1611 cm^{-1}. This low frequency, 26 cm^{-1} lower than in the monomer, is consistent with the double acceptor nature of the carbonyl group, with calculated H-bond distances between the C═O, and NH/OH groups of 1.755/1.830 Å, respectively. Upon electronic excitation the NH_2 bend frequency follows that of the monomer, shifting down 82 cm^{-1} to 1552 cm^{-1}, nearly identical to that in MA monomer. This is further evidence that in both S_0 and S_1 electronic states the amine group is largely unperturbed by the water molecule, consistent with the assigned structure in which the H_2O molecule binds to C═O from the ester pocket (Fig. 1b).

Finally, in the ground state, the H_2O bend fundamental appears at 1620 cm^{-1}, a value close to that in free H_2O (1595 cm^{-1}). However, in the S_1 state spectrum (Fig. 7b), we tentatively assign the transition at 1635 cm^{-1} to the bend fundamental based on comparison with calculations. A value this high in frequency reflects a substantial strengthening of the H-bond between H_2O and MA in the S_1 state. This shift to higher frequency upon strengthening of the intermolecular hydrogen

Table 2 Select experimental and calculated frequencies in MA–H_2O

S_0			S_1		
Exp./cm^{-1}	Calc./cm^{-1}	Assignment	Exp./cm^{-1}	Calc./cm^{-1}	Assignment
3725	3731[b] (3725[a])	H_2O AS stretch	3721	3723[b] (3717[a])	H_2O AS stretch
3569	3563[b] (3534[a])	H_2O SS stretch	3516	3483[b] (3441[a])	H_2O SS stretch
3543	3541[b] (3539[a])	NH_2 AS stretch	3460	3487[b] (3484[a])	'Free' NH stretch
3405	3396[b] (3398[a])	NH_2 SS stretch	—	3072[b] (3072[a])	'Dislocated' NH stretch
—	3188[b]	H_2O bend overtone	3196	3196[b]	H_2O bend overtone
3036	3040[b] (3026[a])	CH_3 FR	3022	3022[b] (3008[a])	CH_3 FR
3012	3016[b] (3002[a])	CH_3 FR	2995	2988[b] (2973[a])	CH_3 FR
2966	2964[b] (2929[a])	CH_3 FR	2958	2955[b] (2909[a])	CH_3 FR
2922	2927[b]	CH_3 FR	2914	2929[b]	CH_3 FR
—	2921[b]	CH_3 FR	2910	2921[b]	CH_3 FR
2908	2904[b]	CH_3 FR	—	2904[b]	CH_3 FR
—	2901[b]	CH_3 FR	—	2898[b]	CH_3 FR
—	2888[b]	CH_3 FR	—	2883[b]	CH_3 FR
2865	2847[b]	CH_3 FR	2853	2841[b]	CH_3 FR
1702	1690[a]	C═O stretch	1611	1615[a]	C═O stretch
1634	1634[a]	NH_2 bend	1548	1548[a]	NH_2 bend
1620	1616[a]	H_2O bend	1636	1632[a]	H_2O bend

[a] Scaled harmonic frequency. [b] Frequency from local mode model.

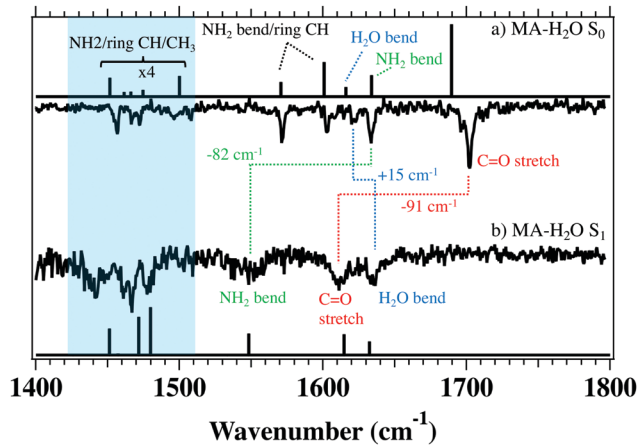

Fig. 7 (a) Ground and (b) S_1 excited state RIDIR spectra from 1400–1800 cm^{-1} of methyl anthranilate–H_2O. The calculated scaled harmonic normal mode frequencies (black stick spectra) are compared with experiment. See text for further discussion.

bond is consistent with the analogous hydrogen bond donor H_2O bend frequency in the water dimer of 1629 cm^{-1}.[30] This change in vibrational frequency is a response to the shifting electron density of the MA monomer, where vertical TD-DFT calculations indicate increasing electron density and negative charge on the carbonyl oxygen upon electronic excitation, thereby making it a better hydrogen bond acceptor. The change in electrostatic potential mapped onto the surface of increasing electron density in going from S_0 to S_1 is presented in Fig. S1 (ESI†), and shows nearly identical features to that of the monomer (Fig. 5), *i.e.*, increasing electron density/negative charge on the carbonyl oxygen at the expense of loss of electron density/negative charge on the nitrogen atom.

V. Discussion

With the aid of a combination of anharmonic models based on a local mode Hamiltonian and DFT calculations, we have assigned all experimental bands in the high-frequency IR spectrum of MA and MA–H_2O in both the S_0 and S_1 electronic states. In the excited state, normal mode calculations predict the uncoupling of the NH_2 group vibrations into localized NH stretches of the free and H-bonded NH groups. In both the monomer and water complex, the transition associated with the 'free' NH stretch is firmly assigned to the band at 3457 and 3461 cm^{-1}, respectively. The vibrational transition associated with the hydrogen bonded 'dislocated' NH stretch is calculated to lie $\sim$500 cm^{-1} lower in frequency and have an intensity more than 10 times that of any other band in the region.

The striking absence of this transition in the spectra of both MA and MA–H_2O requires an explanation. We note that missing IR transitions have been observed previously in excited state IR spectra (*e.g.*, in indole derivatives) due to the presence of a dissociative excited state (*e.g.*, $\pi\sigma^*$) not far above the excited state origin.[31] However, the S_1 state of MA is well isolated from other excited states, and there is no evidence for such a mechanism being at play. Table S1 (ESI†) presents the calculated seven lowest energy electronic states in MA and MA–H_2O. As a result, the missing NH stretch fundamental in MA stimulated development of the theoretical models outlined in Section III.B. In what follows, we describe the results of the adiabatic modelling of the NH stretch vibration of the MA monomer in the ν_{NH} = 0 and 1 states of the H-bonded, 'dislocated' NH stretch transition with an eye toward explaining this striking anomaly.

We focus attention in this section on the NH stretch adiabatic calculations. To that end, we minimized the NH(D) stretch ν_{NH} = 0 and ν_{NH} = 1 energies on the S_0 and S_1 surfaces as a function of select coordinates. Of the 54 internal coordinates, 32 were constrained to their equilibrium values. The 6 carbon atoms and 4 hydrogen atoms of the substituted phenyl ring were held rigid. In addition, the internal coordinates of the methyl group, with the exception of its torsional motion, were constrained. The NH(D) stretch is treated quantum mechanically, while the remaining internal coordinates were allowed to vary.

Fig. 8 compares results for the ν = 0 and ν = 1 NH stretch levels on the S_1 (upper) and S_0 surfaces. These results are obtained with 27 DVR points along the NH stretch, but results obtained for 17 points were similar. The red potential curves correspond to *ab initio* energies obtained by varying the NH internal coordinate while keeping all remaining coordinates fixed. Shown in Fig. 8a, the minimum in the ν_{NH} = 0 S_1 potential curve is 99 cm^{-1} with respect to the global potential minimum. The zero-point energy of the NH stretch with respect to the latter minimum is E_0 = 1618 cm^{-1}, and the energy of the ν_{NH} = 1 state is 4542 cm^{-1}. In contrast, in Fig. 8b the minimum energy of the S_1 NH stretch potential is 1202 cm^{-1} and the energy of the ν_{NH} = 1 state with respect to the global minimum is E_1 = 3900 cm^{-1}. By varying the remaining internal coordinates in a minimization procedure, we have reduced the total energy of this state by E_s = 642 cm^{-1}. The driving force for the structural change is due to the fact that at the geometry of Fig. 8b, the energy of the NH stretch fundamental transition is only 1604 cm^{-1}.

The analogous curves for the S_0 state are shown in Fig. 8c and d, from which it is apparent that the change in structure upon NH stretch excitation is much reduced. For ν_{NH} = 1 we find that E_s = 34 cm^{-1}. This contrast between S_0 and S_1 states makes clear the unusual effects present in the S_1 state, which are largely absent in the S_0 state, despite the presence of a significant NH$\cdots$O=C H-bond there as well.

The biggest changes in the internal coordinates correspond to out-of-plane displacements of both the O and H involved in the enhanced H-bonding. Both atoms move in the same out-of-plane direction with changes in dihedral angles of 9° and 8°, respectively, from the planar equilibrium structure. As such there are two equivalent minima structures. A similarly large change occurs in the H-bonded HNC angle, which decreases from 116.2° to 108.5°. In the language of electronic transitions, this leads to a vertical transition energy that is 642 cm^{-1} greater than the energy difference corresponding to the minima. The large energetic relaxation indicates that the infrared oscillator

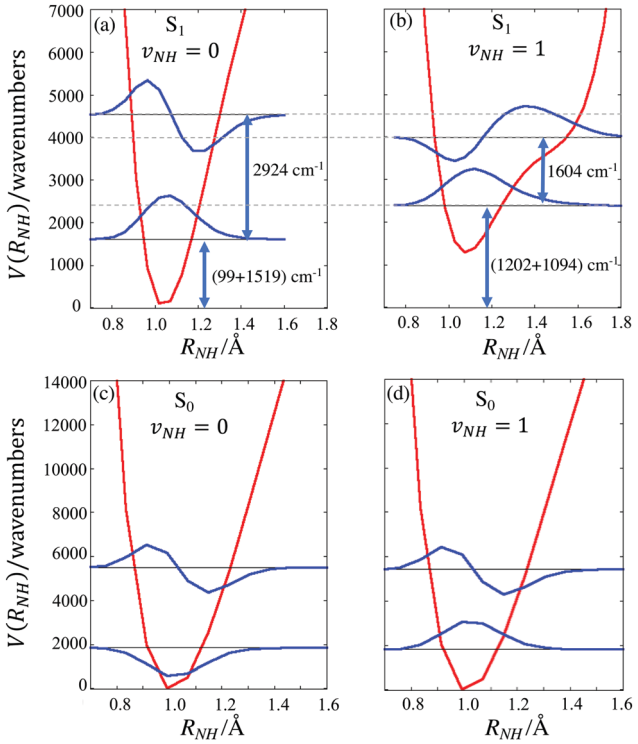

Fig. 8 (a) and (b) Show the two lowest energy NH stretch eigenfunctions and corresponding potentials in S_1 plotted as a function of bond length. The zero of energy is the true calculated potential minimum of the excited state. Remaining coordinates values were chosen to minimize $E(v = 0)$ in (a) and $E(v = 1)$ in (b). In (a) there is 99 cm^{-1} of energy at the bottom of the well; in (b) there is 1202 cm^{-1} of energy. In (a) $E(v = 0)$ is 1618 cm^{-1} and $E(v = 1)$ is 4542 cm^{-1}. In (b) $E(v = 0)$ is 2296 cm^{-1} and $E(v = 1)$ is 3900 cm^{-1}. The energy difference between 4542 and 3900 cm^{-1} will get deposited into the remaining degrees of freedom. Results are for excited states using the TD/B3LYP/6-311++(d,p) level of theory with dispersion. (c) and (d) Show analogous results for the S_0 electronic state. In both plots all coordinates but the NH stretch internal coordinate are held fixed. The NH stretch coordinate is varied to obtain the potential (red) and the associated wave functions.

strength anticipated to be in a single NH stretch transition will be spread over many transitions spanning more than 1000 cm^{-1}, with long progressions arising from vibrational Franck–Condon factors involving several internal coordinates. The center of the transition frequency would correspond to the energy of the vertical transition which is 2924 cm^{-1}, but the lowest possible transition energy would be 642 cm^{-1} less.

The extent of the H atom dislocation on the S_1 surface that occurs upon vibrational excitation can be quantified using the wavefunction shown in Fig. 8b, if we consider the O–H distance that corresponds to each N–H distance. When R_{NH} is 1.28 Å the H atom is equidistant between the N and the O atoms. For the $v_{NH} = 1$ wavefunction, the expectation value of R_{NH} is 1.30 Å, a value slightly greater, so the adiabatic model predicts that the H atom is on average slightly closer to the O atom than the N atom.

While the current experimental study does not address isotopic effects, it is worthwhile to consider how these results might change in ND_2 compared to NH_2. As shown in Fig. S2c and d (ESI†), the analogous structural rearrangement calculated to occur upon ND stretch excitation is substantially less dramatic. The difference between the vertical and minimum energies for the $v_{ND} = 1$ state is $E_s = 151$ cm^{-1} compared to the analogous 642 cm^{-1} value found for the NH stretch.

In order to examine the combined effects of the stretch and the bend we show the potential surface as a function of these two modes in Fig. 9a. The remaining coordinates are constrained to the geometry that minimizes the $v_{NH} = 0$ state following the procedure described above. The equipotential energy contours (every 1000 cm^{-1}) indicate that the NH stretch is strongly coupled to the bend, with the stretch potential being qualitatively different for the two slices at θ_{HNC} = 1.8 and 2.2 radians. The four lowest energy eigenfunctions, along with their associated eigenvalues are displayed in Fig. 9(b–e). The excitation energy of the NH stretch fundamental is calculated to be 2634.7 cm^{-1}.

In order to gauge the role of the potential anharmonicity, we repeat the calculation with the same kinetic energy operator but assume a quadratic potential obtained from a Taylor series for these two degrees of freedom at the $v_{NH} = 0$ geometry. These analogous plots are displayed in Fig. 9(f–j). We obtain an NH stretch fundamental transition energy of 3128.6 cm^{-1}. That value is similar to the 3190.7 cm^{-1} value obtained from a normal mode calculation obtained at the global minimum, indicating that the very large shifts are due to the unusually large anharmonicity of the potential shown in Fig. 9a. Fig. 9 also includes the results of intensity calculations. The results (given in km mol^{-1}) shown indicate that for the NH fundamental the linear dipole leads to an intensity of $I_L = 331$ km mol^{-1} *versus* 497 km mol^{-1} for the dipole evaluated at the DVR grid of points.

The purpose of the stretch–bend model is to show that the bending motion is strongly coupled to the NH stretch. These results are not to be directly compared to experiment, since the bend itself is strongly coupled to other modes. Indeed, at least 12 calculated normal modes display significant HNC bend character, with many other vibrations at similar frequencies to that of the bend. There are also other modes directly coupled to the NH stretch.

The above two calculations suggest that the NH stretch fundamental should be strongly coupled to other degrees of freedom and that the intensity of the mode should be broadly distributed amongst several transitions spread over several hundred wavenumbers. Perhaps the low-intensity, diffuse bands seen near 2800 cm^{-1} (Fig. 3b) and in AA at 2900 cm^{-1} can be ascribed to some of these features. As noted above, this effect would not be accounted for in VPT2 calculations. This suggests that a restricted, rectilinear, quartic potential is unlikely to capture the key features of the potential shown in Fig. 9a. This is not too surprising given its shape; a low order Tayler series expansion cannot be expected to capture the valley that appears as the HNC angle is reduced from its equilibrium configuration. The shape of this valley indicates that orientation plays a critical role in the H-atom dislocation; only when the bend angle decreases to about 1.8 rad is there a low energy pathway for this dislocation.

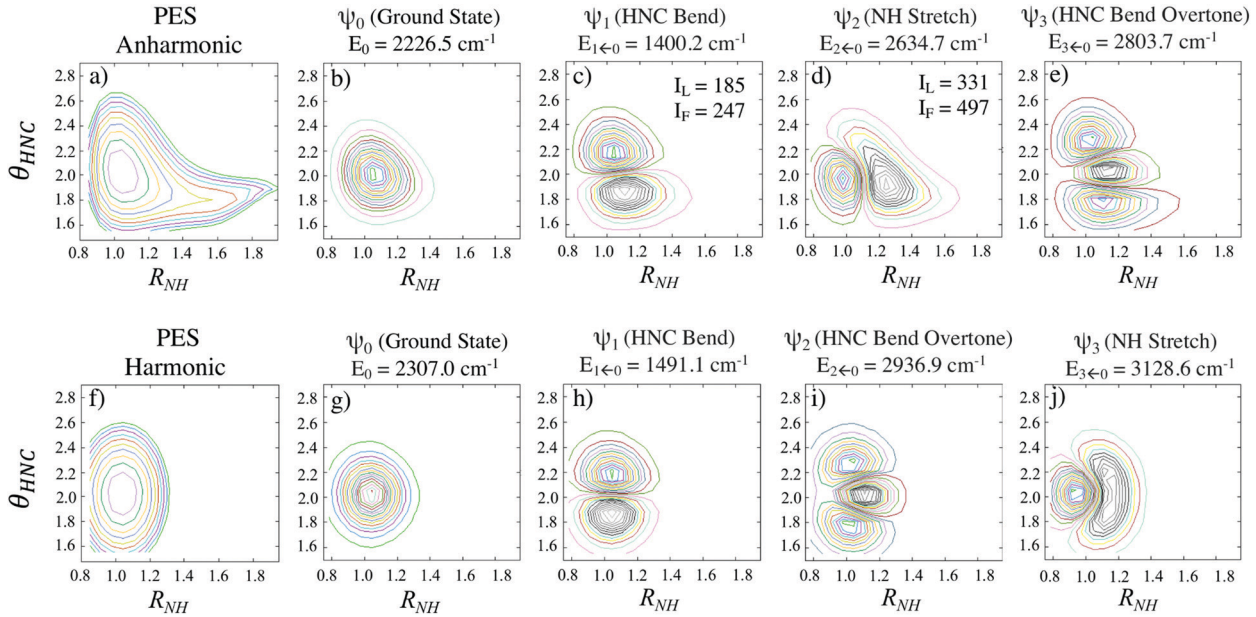

Fig. 9 Equipotential curves plotted every 1000 cm^{-1} as a function of NH stretch and HNC bend coordinates. The remaining coordinates are constrained to the geometry that minimizes the v_{NH} = 0 state following the adiabatic procedure described in the text. (a) Displays the anharmonic calculated potential energy surface and (b)–(e) show the four corresponding lowest energy eigenfunctions along with their associated eigenvalues. Intensities (km mol^{-1}) are given for select transitions using a linear dipole (I_L) and full dipole (I_F), the latter of which is evaluated at the DVR grid of points. (f)–(j) Show analogous plots obtained with a quadratic potential from a Taylor series for the two degrees of freedom at the v_{NH} = 0 geometry. See text for further discussion.

VI. Conclusions

We have postulated that the apparent absence of a transition ascribable to the NH stretch of the H-bonded, 'dislocated' NH group in the S_1 state of MA and MA–H_2O is the result of an extreme instance of anharmonic mixing involving the NH stretch and the HNC bend. Using an adiabatic vibrational model involving the NH stretch, we have demonstrated that this absorption will have its oscillator strength spread over transitions spanning hundreds of wavenumbers. If these transitions are in turn broadened by strong coupling with other background states, the result will be a broad, low-intensity band that is hard to observe, consistent with experiment. Since observation of a structured background could add further insight to the pre-reactive H-atom transfer process, future studies that can detect it with good sensitivity are still needed. Alternatively, analogous studies of the ND_2 MA isotopomer would also confirm the model, as we predict a significant reduction in the effects there.

It is interesting to compare the current NH stretch results on the S_1 surface with the observed OH stretch spectrum of benzoic acid dimer.[32] In the latter system there is especially strong hydrogen bonding that profoundly affects the IR spectrum leading to an intense absorption centered around 2900 cm^{-1} with features spanning 600 cm^{-1}. Despite its breadth, this feature completely dominates this region of the IR spectrum, a situation that starkly contrasts with the disappearance of the NH stretch band. Comparing the intensities of the associated normal NH and OH stretches we find I_{NH} = 420 km mol^{-1} for the former and I_{OH} = 6692 km mol^{-1} for the latter using the B3LYP hybrid functional in conjunction with Grimme's dispersion correction (version D3),[19] Becke–Johnson damping,[20] and the def2TZVP basis set. We believe that this large intensity difference combined with the NH stretch spectral features being predicted to spread over twice the spectral range, are key factors that lead to dramatically different spectra.

Finally, it seems likely that a similar strong stretch–bend coupling is present in other molecules that engage in excited-state keto–enol tautomerisation, including salicylic acid. Indeed, the H-bonded OH stretch has not been identified in the S_1 state of SA and its derivatives, suggesting that a similar mechanism may be in operation.[11,33,34] The time-dependent development of the infrared spectra in the anthranilate and salicylate derivatives is worth future effort.

Conflicts of interest

There are no conflicts to declare.

Appendix

In this Appendix we review the localization scheme used in this work. We refer to the localized coordinates as localized normal coordinates as these coordinates are obtained directly from the normal coordinates $\boldsymbol{Q}$ *via* an orthogonal transformation, $\boldsymbol{R} = \boldsymbol{AQ}$.

The matrix $\boldsymbol{A}$ is constructed in several steps. Using the stretches as an example, if there are N CH stretches, there will also be N normal modes that are predominantly admixtures of these CH stretches. Typically, these modes have frequencies

that span a narrow enough frequency range that no other molecular motions contribute to these normal modes. We find a localized mode, associated with each CH stretch by carrying out a normal mode calculation in which all the H atom masses are increased by a factor c, except for the H mass of the CH being localized. This mass retains its original value. In this calculation there will be a single normal mode that corresponds to a localized CH stretch. The process is repeated for each of the N stretches in order to find N CH localized normal modes, $\boldsymbol{Q}'$. These modes are expressed as linear combinations of the 10 original normal coordinates $\boldsymbol{Q}' = \boldsymbol{LQ}$ with minor contributions from lower frequency modes.

Since the rows of $\boldsymbol{L}$ are calculated from distinct normal mode calculations, this matrix is not orthogonal. It can be well approximated as an orthogonal matrix as follows. Calculating the overlap $\boldsymbol{S} = \boldsymbol{L}^{\mathrm{T}}\boldsymbol{L}$ and solving for $\boldsymbol{S}^{-1/2}$ we find the desired localized coordinates $\boldsymbol{R} = \boldsymbol{LS}^{-1/2}\boldsymbol{Q} \equiv \boldsymbol{AQ}$ that describe the CH stretch vibrations. The resulting Hamiltonian is given by eqn (1).

Acknowledgements

KNB, JLF, and TSZ gratefully acknowledge support for this research by the National Science Foundation under grant CHE-1764148. ELS gratefully acknowledges support from NSF *via* Grant No. CHE-1566108.

References

1 T. N. Karsili, B. Marchetti, M. N. Ashfold and W. Domcke, *J. Phys. Chem. A*, 2014, **118**, 11999–12010.
2 A. L. Sobolewski and W. Domcke, *Phys. Chem. Chem. Phys.*, 2006, **8**, 3410–3417.
3 P. B. Bisht, H. Petek, K. Yoshihara and U. Nagashima, *J. Chem. Phys.*, 1995, **103**, 5290–5307.
4 Y. Peperstraete, M. Staniforth, L. A. Baker, N. D. N. Rodrigues, N. C. Cole-Filipiak, W.-D. Quan and V. G. Stavros, *Phys. Chem. Chem. Phys.*, 2016, **18**, 28140–28149.
5 L. A. Baker, M. D. Horbury, S. E. Greenough, P. M. Coulter, T. N. Karsili, G. M. Roberts, A. J. Orr-Ewing, M. N. Ashfold and V. G. Stavros, *J. Phys. Chem. Lett.*, 2015, **6**, 1363–1368.
6 N. D. Rodrigues, M. Staniforth and V. G. Stavros, *Proc. R. Soc. A*, 2016, **472**, 20160677.
7 L. A. Baker, B. Marchetti, T. N. Karsili, V. G. Stavros and M. N. Ashfold, *Chem. Soc. Rev.*, 2017, **46**, 3770–3791.
8 L. Heimbrook, J. E. Kenny, B. E. Kohler and G. W. Scott, *J. Phys. Chem.*, 1983, **87**, 280–289.
9 L. A. Heimbrook, J. E. Kenny, B. E. Kohler and G. W. Scott, *J. Chem. Phys.*, 1981, **75**, 5201–5203.
10 C. A. Southern, D. H. Levy, G. M. Florio, A. Longarte and T. S. Zwier, *J. Phys. Chem. A*, 2003, **107**, 4032–4040.
11 A. L. Sobolewski and W. Domcke, *J. Phys. Chem. A*, 2004, **108**, 10917–10922.
12 F. Egidi, D. B. Williams-Young, A. Baiardi, J. Bloino, G. Scalmani, M. J. Frisch, X. Li and V. Barone, *J. Chem. Theory Comput.*, 2017, **13**, 2789–2803.
13 K. N. Blodgett, D. Sun, J. L. Fischer, E. L. Sibert and T. S. Zwier, *Phys. Chem. Chem. Phys.*, 2019, **21**, 21355–21369.
14 P. Kolek, M. Andrzejak, R. Hakalla and W. Szajna, *J. Phys. Chem. A*, 2018, **122**, 6243–6255.
15 C. A. Arrington, C. Ramos, A. D. Robinson and T. S. Zwier, *J. Phys. Chem. A*, 1998, **102**, 3315–3322.
16 F. A. Ensminger, J. Plassard, T. S. Zwier and S. Hardinger, *J. Chem. Phys.*, 1995, **102**, 5246–5259.
17 T. S. Zwier, *J. Phys. Chem. A*, 2001, **105**, 8827–8839.
18 M. Frisch, G. Trucks, H. Schlegel, G. Scuseria, M. Robb, J. Cheeseman, G. Scalmani, V. Barone, G. Petersson and H. Nakatsuji, *Gaussian 16, Revision A*, 2016.
19 S. Grimme, *J. Comput. Chem.*, 2004, **25**, 1463–1473.
20 S. Grimme, *J. Chem. Phys.*, 2006, **124**, 034108.
21 E. L. Sibert, D. P. Tabor, N. M. Kidwell, J. C. Dean and T. S. Zwier, *J. Phys. Chem. A*, 2014, **118**, 11272–11281.
22 D. Luckhaus, *J. Chem. Phys.*, 2000, **113**, 1329–1347.
23 E. B. Wilson, J. C. Decius and P. C. Cross, *Molecular vibrations: the theory of infrared and Raman vibrational spectra*, Courier Corporation, 1980.
24 T. Nakanaga, F. Ito, J. Miyawaki, K. Sugawara and H. Takeo, *Chem. Phys. Lett.*, 1996, **261**, 414–420.
25 E. L. Sibert, W. P. Reinhardt and J. T. Hynes, *Chem. Phys. Lett.*, 1982, **92**, 455–458.
26 J. M. Bakker, L. Mac Aleese, G. von Helden and G. Meijer, *J. Chem. Phys.*, 2003, **119**, 11180–11185.
27 S. Stepanian, I. Reva, E. Radchenko and G. Sheina, *Vib. Spectrosc.*, 1996, **11**, 123–133.
28 H. Piest, G. von Helden and G. Meijer, *J. Chem. Phys.*, 1999, **110**, 2010–2015.
29 M. Mukherjee, B. Bandyopadhyay, P. Biswas and T. Chakraborty, *Indian J. Phys.*, 2012, **86**, 201–208.
30 J. Paul, R. Provencal, C. Chapo, K. Roth, R. Casaes and R. Saykally, *J. Phys. Chem. A*, 1999, **103**, 2972–2974.
31 B. C. Dian, A. Longarte and T. S. Zwier, *J. Chem. Phys.*, 2003, **118**, 2696–2706.
32 G. Florio and T. Zwier, *J. Chem. Phys.*, 2003, **118**, 1735.
33 T. Yahagi, A. Fujii, T. Ebata and N. Mikami, *J. Phys. Chem. A*, 2001, **105**, 10673–10680.
34 E. A. E.-H. A. El, A. Fujii, T. Ebata and N. Mikami, *Chem. Phys. Lett.*, 2003, **376**, 788–793.